
CONFORMALIZED LATE FUSION MULTI-VIEW LEARNING

Eduardo Ochoa Rivera*

Department of Statistics
University of Michigan
Ann Arbor, MI 48104
eochoa@umich.edu

Yash Patel**

Department of Statistics
University of Michigan
Ann Arbor, MI 48104
yppatel@umich.edu

Ambuj Tewari

Department of Statistics
University of Michigan
Ann Arbor, MI 48104
tewaria@umich.edu

ABSTRACT

Uncertainty quantification for multi-view learning is motivated by the increasing use of multi-view data in scientific problems. A common variant of multi-view learning is late fusion: train separate predictors on individual views and combine them after single-view predictions are available. Existing methods for uncertainty quantification for late fusion often rely on undesirable distributional assumptions for validity. Conformal prediction is one approach that avoids such distributional assumptions. However, naively applying conformal prediction to late-stage fusion pipelines often produces overly conservative and uninformative prediction regions, limiting its downstream utility. We propose a novel methodology, Multi-View Conformal Prediction (MVCP), where conformal prediction is instead performed separately on the single-view predictors and only fused subsequently. Our framework extends the standard scalar formulation of a score function to a multivariate score that produces more efficient downstream prediction regions in both classification and regression settings. We then demonstrate that such improvements can be realized in methods built atop conformalized regressors, specifically in robust predict-then-optimize pipelines.

1 Introduction

Multi-view machine learning is becoming increasingly common with the advent of multi-modal language models and conditional generative models [1, 2, 3, 4, 5]. In addition, such techniques are being increasingly used in more safety-critical settings, such as medicine [6, 7, 8, 9] and robotics [10, 11, 12, 13]. These use cases motivate the development of uncertainty quantification methods for multi-view learning.

The most common division of multi-view learning is along the axis of *when* fusion of the multiple views is performed. We can either learn a fused *data* representation or we can fuse the *predictions* from the separate views. The latter approach is referred to as “late fusion”. It is desirable in limited resource settings, where the separately trained models can be combined in a light-weight fashion for downstream tasks [14, 15, 16, 17]. Increasing interest is now being placed on quantifying uncertainty for such models [18, 19, 20, 21, 22]. Such methods, however, rely on distributional assumptions to provide coverage guarantees or are computationally intractable, limiting their practical utility. These limitations, therefore, demand a more universal, yet informative, uncertainty quantification method.

One such method for performing distribution-free uncertainty quantification is conformal prediction, which provides a principled framework for producing distribution-free prediction regions with marginal frequentist coverage guarantees [23, 24]. By using conformal prediction on a user-defined score function $s(x, y)$ and obtaining an empirical $1 - \alpha$ quantile $\hat{q}(\alpha)$ of $s(x, y)$ over a calibration set \mathcal{D}_C , prediction regions $\mathcal{C}(x) = \{y \mid s(x, y) \leq \hat{q}(\alpha)\}$ attain marginal coverage guarantees. While calibration is guaranteed from this procedure, predictive efficiency, quantified as the size of the resulting prediction regions, can be unboundedly large for poorly chosen score functions.

We extend the conformal prediction line of work to enable its practical use in late-stage multi-view prediction problems. In particular, we propose a multivariate extension to the score function notion introduced in traditional conformal prediction, with a corresponding extension of quantiles to “quantile envelopes.” We demonstrate that this formulation

*Denotes alphabetic ordering indicating equal contributions.

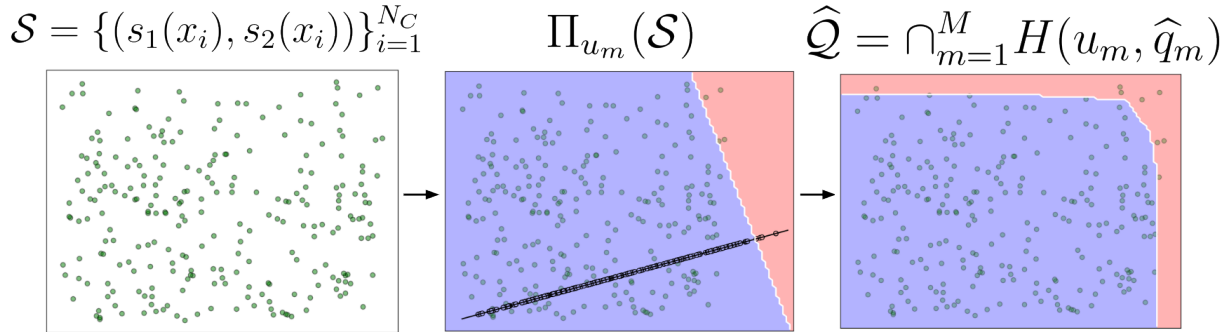


Figure 1: MVCP provides a principled extension to the standard conformal prediction pipeline by leveraging ideas from higher-dimensional quantile regression to define quantile envelopes $\hat{\mathcal{Q}}$ instead of purely scalar quantiles \hat{q} . It does so by evaluating a collection of score functions (here s_1 and s_2) over the calibration dataset to define \mathcal{S} , finding quantiles $\{\hat{q}_m\}$ over a set of projection directions $\{u_m\}$, and taking $\hat{\mathcal{Q}}$ to be the intersection of the resulting half-planes $H(u_m, \hat{q}_m)$. These quantile envelopes result in more informative prediction regions that can be used in downstream tasks.

retains the desired distribution-free coverage guarantees typical of standard conformal prediction and that the resulting prediction regions can be used efficiently in both classification and regression settings. Our contributions are:

- Providing a multivariate extension to conformal prediction score functions (MVCP) that retains coverage guarantees and can be applied to late-stage multi-view prediction problems.
- Demonstrating how the resulting prediction regions can be efficiently leveraged for downstream classification and regression tasks.
- Demonstrating the empirical performance of the MVCP framework across a suite of tasks.

2 Background

2.1 Conformal Prediction

Coverage guarantees of uncertainty quantification methods generally rely on distributional assumptions, often via asymptotics or explicit model specification. To alleviate the need for such restrictive assumptions, interest in finite-sample, distribution-free uncertainty quantification methods has risen. Conformal prediction is one such method [23, 24]. Due to its lack of structural assumptions, conformal prediction pairs well with the increasingly common black-box style of modeling.

Conformal prediction serves as a wrapper around such predictors, producing prediction regions $\mathcal{C}(x)$ that have formal guarantees of the form $\mathcal{P}_{X,Y}(Y \notin \mathcal{C}(X)) \leq \alpha$ for some prespecified level α . To achieve this, “split conformal” partitions the dataset \mathcal{D} into a training set \mathcal{D}_T and a calibration set \mathcal{D}_C . The former plays the role traditionally played by \mathcal{D} , namely serving as data used to fit \hat{f} . The latter is used much in the way a validation set is typically employed in practice. Formally, users of conformal prediction must design a “score function” $s(x, y)$, which should quantify “test error,” often in a domain-specific manner. For instance, a simple score function for a regression setting would be $s(x, y) = \|\hat{f}(x) - y\|$. This score function is then evaluated across the calibration set to define $\mathcal{S} = \{s(x, y) \mid (x, y) \in \mathcal{D}_C\}$. For a desired coverage of $1 - \alpha$, we then take \hat{q} to be the $\lceil (|\mathcal{D}_C| + 1)(1 - \alpha) \rceil / |\mathcal{D}_C|$ quantile of \mathcal{S} , with which prediction regions for future test queries x can be defined as $\mathcal{C}(x) = \{y \mid s(x, y) \leq \hat{q}\}$. Under the exchangeability of the score of a test point $s(x', y')$ with \mathcal{S} , we have the desired *finite-sample* probabilistic guarantee that $1 - \alpha \leq \mathcal{P}_{X,Y}(Y \in \mathcal{C}(X))$.

While this guarantee holds for any $s(x, y)$, the informativeness of the resulting prediction regions, formally defined as the inverse expected Lebesgue measure across X , i.e. $(\mathbb{E}[\mathcal{L}(\mathcal{C}(X))])^{-1}$, is intimately tied to its specification [24]. Thus, much of the practical challenge of conformal prediction relates to choosing a score function that retains coverage while minimizing prediction region size.

2.2 Predict-Then-Optimize

Prediction regions produced from conformalized predictors are often leveraged differently across classification and regression settings. In the case of classification, “regions” simply constitute a subset of the label space, making its direct use by end users straightforward, as demonstrated in works such as [25]. In high-dimensional regression settings, however, prediction regions become harder to use directly; for this reason, recent works have started shifting focus to using them in their implicit forms.

One such application is [26], where conformal prediction was leveraged in a predict-then-optimize setting. As the name suggests, predict-then-optimize problems are two-stage problems, which take observed contextual information x and predict the parametric specification of a downstream problem of interest $\hat{c} := g(x)$ with some trained predictor g . The final result is then a decision made with this specification, $w^* := \min_w f(w, \hat{c})$. An example of such a setting is if an optimal labor allocation w^* is sought based on predicted demand \hat{c} from observed transactions x in a food delivery platform.

While the predicted \hat{c} is often simply trusted in the downstream optimization, this approach is inappropriate in risk-sensitive settings, where misspecification of the map $g : \mathcal{X} \rightarrow \mathcal{C}$ could lead to highly suboptimal decision-making. For this reason, recent interest has been placed on studying a “robust” alternative to this formulation [27, 28, 29]. Following this line of work, [26] proposed studying the following formulation: $w^*(x) := \min_w \max_{\hat{c} \in \mathcal{C}(x)} f(w, \hat{c})$, with the uncertainty region $\mathcal{C}(x)$ being produced by conformalizing the predictor g . The primary consequence of doing so was having a probabilistic guarantee on the suboptimality gap. That is, denoting the suboptimality gap by $\Delta(x, c) := \min_w \max_{\hat{c} \in \mathcal{C}(x)} f(w, \hat{c}) - \min_w f(w, c)$, where c is the true parameter corresponding to x , they established that leveraging conformal uncertainty regions guarantees $\mathcal{P}_{X, \mathcal{C}}(0 \leq \Delta(X, C) \leq L \text{diam}(\mathcal{C}(X))) \geq 1 - \alpha$ if $f(w, c)$ is an objective function that is convex-concave and L -Lipschitz in c for any fixed w .

2.3 Multi-View Learning

We provide a brief overview of multi-view learning herein, deferring to recent surveys of the field for a more comprehensive review thereof [30]. In general, the focus of multi-view machine learning is to solve prediction problems when different, often non-overlapping, representations of the same underlying “object” are observed. Methods in this space bifurcate between those defined together with some downstream supervised task and those seeking to find an abstract “fused” representation that lends itself naturally for arbitrary downstream use cases. We focus herein on the former category. For instance, one may wish to classify a captioned image, where the image and caption represent two distinct “views” of the same underlying abstract object in this case.

Formally, therefore, we consider the multi-view prediction problem as seeking a map $\mathcal{X} \rightarrow \mathcal{Y}$ with $\mathcal{X} = \mathcal{X}_1 \cup \dots \cup \mathcal{X}_K$. As previously mentioned, fusion approaches are generally either early-stage or late-stage. In the former, we seek to learn some common, often abstract, space into which these separate views can be mapped for downstream prediction, namely seeking a map g_ϕ that maps $g_\phi : \mathcal{X}_1 \times \dots \times \mathcal{X}_K \rightarrow \mathcal{Z}$. Such a fusion map is then assumed to be usable for the downstream prediction task, namely through composition with $f_\theta : \mathcal{Z} \rightarrow \mathcal{Y}$ such that the overall prediction model can be defined as $f \circ g$. Traditionally, g was hand-crafted, leveraging domain-specific insights. However, increasingly, f and g are simply subsets of a neural network trained end-to-end via gradient descent, such as in [31, 32, 33, 34, 35, 36].

As discussed previously, this fusion approach is not universally desirable in all circumstances though, such as when models for individual views have already been curated after computationally intensive training and hyperparameter tuning [14, 15, 16, 17]. In such cases, late-stage fusion approaches can be preferred, where separate predictors $f_i : \mathcal{X}_i \rightarrow \mathcal{Y}$ have been trained and are fused via a post-hoc algorithm $\mathcal{F} : \mathcal{Y} \times \dots \times \mathcal{Y} \rightarrow \mathcal{Y}$. Approaches to this include decision averaging [37, 38], decision weighting [18, 39, 40], and decision voting [41]. We focus herein on such late-stage fusion.

2.4 Related Works

Work in the conformal prediction literature has yet to leverage the generalized notions of quantiles considered herein. Generalizations of quantiles, while introduced first in the context of conformal prediction herein, have a long history in traditional statistics, with recent surveys on approaches available in [42, 43]. We briefly summarize the relevant pieces of this literature below.

Unlike univariate data, multivariate data does not lend itself to an unambiguous definition of a quantile, as there is no canonical ordering of points in higher dimensional spaces. To account for this, one class of multivariate quantiles, known as “directional quantiles,” prescribes directions along which data points can be compared [44, 45, 46]. That is, for some direction $u \in \mathcal{S}^{n-1}$, points $x \in \mathbb{R}^n$ are projected, after which the standard notion of a quantile can be leveraged.

The notion of the α quantile for a random variable $X \in \mathcal{X}$ clearly then depends on this choice of direction u , which we denote by $Q(X, \alpha, u) = \inf\{q \in \mathbb{R} : \mathcal{P}(u^\top X \leq q) \geq \alpha\}$. When there is no ambiguity, we just denote it as $Q(\alpha, u)$. In cases where domain knowledge assigns an unambiguous notion of multivariate ordering, such knowledge can be encoded into the choice of u . In other cases, however, a more agnostic approach is typically employed: rather than choosing any particular direction, all directions are considered simultaneously. Formally, for any given u , notice the choice of quantile defines a corresponding halfplane $H(u, Q(\alpha, u)) = \{x \in \mathcal{X} : u^\top x \leq Q(\alpha, u)\}$. To extend this to consider all directions simultaneously, we then define the quantile envelope to be

$$D(\alpha) = \bigcap_{u \in \mathcal{S}^{n-1}} H(u, Q(\alpha, u)). \quad (1)$$

To the best of our knowledge, the only work leveraging conformal prediction in the context of multivariate quantiles is [47]. This work, however, focuses on a fundamentally different problem than that considered herein. In particular, they focused on *leveraging* conformal prediction as a correction step to the output of directional quantile regression with the intended use case being in constructing calibrated prediction regions for multivariate regression problems. This work, therefore, was a natural extension to the now classical application of conformal prediction for the correction of univariate quantile regression. Our proposed method, however, does the converse: it leverages directional quantiles *within the score space* to extend conformal prediction itself.

3 Method

We now introduce a procedure for uncertainty quantification for late-stage fusion. We discuss the naive approach in Section 3.1 and its extension along with the associated coverage guarantees in Section 3.2. We then discuss the downstream use of the resulting prediction regions in Section 3.3.

3.1 Naive Approach

We now consider the setting described in the background section, where K predictors f_1, \dots, f_K are trained on the separate views with a late fusion algorithm \mathcal{F} , which we assume to be fixed throughout this presentation. Note that the validity of the results presented below is independent of the predictive quality of such f_i . The efficiency, however, is highly dependent on it. In the standard application of conformal prediction, a score function $s(\mathcal{F}(x), y)$ is defined. For instance, if we assume \mathcal{Y} is some metric space with metric d , as in a regression task, a naive choice of score function would be

$$s(x, y) = d(\mathcal{F}(f_1(x), \dots, f_K(x)), y). \quad (2)$$

Denoting the $\lceil (N_C + 1)(1 - \alpha) \rceil / N_C$ quantile of the score distribution over \mathcal{D}_C as $\hat{q}(\alpha)$, $\mathcal{C}(x) = \{y : s(x, y) \leq \hat{q}(\alpha)\}$ is then marginally calibrated. Ideally, however, prediction regions $\mathcal{C}(x)$ should have the quality that, if a particular predictor has less uncertainty in its predictions, as is frequently true of settings leveraging late-stage fusion, upon routing to that predictor, the corresponding size of the prediction region should be smaller than if it had been routed to a different predictor. While the framing of Equation (2) does, in principle, support this property, it ultimately relies on defining an *uncertainty-aware* late fusion algorithm \mathcal{F} . In its typical form, however, \mathcal{F} simply takes *point predictions* $f_1(x), \dots, f_K(x)$ in as input, meaning any uncertainty-awareness would need to be baked in a priori through domain knowledge of the uncertainties of the predictors f_1, \dots, f_K , which can seldom be specified precisely, in turn sacrificing the downstream predictive efficiency of $\mathcal{C}(x)$.

For this reason, we seek to produce a data-driven approach of obtaining the uncertainties of the predictors by instead fusing the *conformalized* predictors. In this case, we first define a score function s_i for each predictor f_i . For any x , therefore, we now have a multivariate score $s(x, y) := (s_1(x, y), \dots, s_K(x, y))$. A naive approach would then involve leveraging standard conformal prediction over a pre-defined map $g : \mathbb{R}^K \rightarrow \mathbb{R}$, e.g., $g(s) = \sum_{k=1}^K s_k$. As in the case of conformalizing the fused predictor directly, using a *fixed* g fails to adapt to any disparities in uncertainties present across predictors or requires intimate knowledge of such uncertainties. We instead wish to provide a data-adaptive pipeline to automatically produce such a g . Formally, denoting by $\mathcal{C}(g) : \mathcal{X} \rightarrow \mathcal{Y}$ the conformalized predictor resulting from calibrating with the score fusion function g in some function class \mathcal{G} , the goal can be formulated as seeking $g^* := \arg \min_{g \in \mathcal{G}} \mathbb{E}_X [\mathcal{L}(\mathcal{C}(g)(X))]$. There is, however, no approach to solving this abstract formulation, since even the mere evaluation of $\mathbb{E}_X [\mathcal{L}(\mathcal{C}(g)(X))]$ for a fixed g is intractable.

3.2 MVCP: Score Quantile Envelope

Since finding g^* exactly is intractable, we propose a data-adaptive approach that leverages the notion of quantile envelopes from Section 2.4 over the scores $s \in \mathbb{R}^K$. Importantly, for the remainder of this discussion, we assume

the score functions are non-negative, i.e., $s_k : \mathcal{X} \times \mathcal{Y} \rightarrow \mathbb{R}_+$, which is typically the case as the score serves as a generalization of the classical idea of a residual. Intuitively, the coverage guarantee in this multivariate extension requires us to define a pre-ordering \lesssim over \mathbb{R}^K , where we only lose the antisymmetric axiom of a total ordering. Upon defining such a pre-ordering, the coverage guarantee follows in using the appropriate quantile under this modified sorting.

Crucially, however, the problem of choosing this pre-ordering closely parallels that of choosing g^* , where a poorly chosen pre-ordering will result in overly conservative quantile envelopes and, hence, prediction regions. For instance, using a lexicographical ordering \lesssim_{Lex} will result in axis-aligned hyper-rectangular quantile regions and similarly a norm-based ordering \lesssim_{Norm} , defined as $s_1 \lesssim_{\text{Norm}} s_2 \iff \|s_1\|_2 \leq \|s_2\|_2$, in hyperspherical regions. Rather than explicitly prescribing a pre-ordering, \lesssim can be implicitly defined by prescribing an indexed family of nested sets $\{\mathcal{A}_t\}_{t \in \mathbb{R}}$, such that $\mathcal{A}_{t_1} \subset \mathcal{A}_{t_2}$ for $t_1 \leq t_2$. We then define \lesssim by stating $s_1 \lesssim s_2$ if $\forall t, s_2 \in \mathcal{A}_t \implies s_1 \in \mathcal{A}_t$.

While not strictly necessary, we restrict ourselves to the case where \mathcal{A}_t is a family of sets defined by a fixed ‘‘base contour’’ that scales outward with t . Under this restriction, performing a comparison of $s_1, s_2 \in \mathbb{R}^K$ in the aforementioned fashion, i.e. checking if $s_1 \lesssim s_2$, amounts to checking if $t(s_1) \leq t(s_2)$, where $t(s)$ is the t for which \mathcal{A}_t ‘‘intersects’’ s . Notably, $t(s)$ is precisely the aforementioned data-driven score fusion function $g(s)$ of interest. Defining a data-adaptive $g(s)$, therefore, reduces to having a data-driven approach for defining the base contour of \mathcal{A}_t . We additionally restrict this base contour to be a convex set; if such a set were permitted to be nonconvex, computing $t(s) := \min\{t \in \mathbb{R} : s \in \mathcal{A}_t\}$ would potentially be computationally expensive, increasing the difficulty in defining the resulting prediction regions. As demonstrated in Section 3.3, many downstream applications require such efficient computation and, hence, benefit from this restriction to convex sets.

To have tight quantile regions, we formally wish for the pre-ordering to have the property that the quantile region given by $\tilde{\mathcal{Q}} := \{s \mid s \lesssim \hat{q}\}$, where \hat{q} is the $1 - \alpha$ empirical quantile of \mathcal{S}_C under \lesssim , should have minimal Lebesgue measure. Notably, by construction, such a $\tilde{\mathcal{Q}}$ will capture $1 - \alpha$ points of \mathcal{S}_C . The problem of discovering an optimal pre-ordering can, thus, be equivalently stated as seeking to define the base contour of \mathcal{A}_t to match that of the tightest $1 - \alpha$ convex cover of \mathcal{S}_C .

This final reframing, therefore, naturally motivates selecting the base contour as the $1 - \alpha$ quantile envelope of \mathcal{S}_C . Using \mathcal{S}_C to define \mathcal{A}_t and in turn \lesssim , however, sacrifices the exchangeability of its points with future test scores s' , as the very nature of ordering would change in swapping s' with any $s \in \mathcal{S}_C$. The goal, then, follows as seeking to define the base contour as the $1 - \alpha$ quantile envelope of \mathcal{S}_C without directly using \mathcal{S}_C . For this reason, we partition $\mathcal{S}_C = \mathcal{S}_C^{(1)} \cup \mathcal{S}_C^{(2)}$, where we define \lesssim using $\mathcal{S}_C^{(1)}$ and compute the final \hat{q} over $\mathcal{S}_C^{(2)}$. Such a split is predicated on the assumption that the $1 - \alpha$ quantile envelope defined over $\mathcal{S}_C^{(1)}$ resembles that of $\mathcal{S}_C^{(2)}$, implying the $|\mathcal{S}_C^{(1)}|$ should be sufficiently large as to capture this structure accurately.

We now focus attention on defining the quantile envelope over $\mathcal{S}_C^{(1)}$, starting by selecting the projection directions $\{u_m\}$. The restriction of s to the positive orthant induces a natural modification of Equation (1), namely where $u \in \mathcal{S}_+^{K-1} := \mathcal{S}^{K-1} \cap \mathbb{R}_+^K$ instead of \mathcal{S}^{K-1} . Exact solution of finding an evenly distributed set of points over hyperspheres in arbitrary n -dimensional spaces is a classically difficult problem [48]. If $K = 2$, we can solve this exactly; for $K > 2$, we generate directions stochastically such that $U \sim \text{Unif}(\mathcal{S}_+^{K-1})$ by drawing $V_1, \dots, V_M \sim \mathcal{N}(0, I^{K \times K})$ and defining $U_i := V_i^{| \cdot |} / \sqrt{V_1^2 + \dots + V_M^2}$, where $v^{| \cdot |}$ denotes the component-wise absolute values of v .

We now wish to define the quantile thresholds $\{\tilde{q}_m\}$ for the selected directions to optimally capture $1 - \alpha$ of $\mathcal{S}_C^{(1)}$. Naively taking the $1 - \alpha$ quantile per projection direction u_m results in *joint* coverage by $\tilde{\mathcal{Q}} := \bigcap_{m=1}^M H(u_m, \tilde{q}_m)$ of $\mathcal{S}_C^{(1)}$ to be $< 1 - \alpha$. To combat this, a straightforward fix is to replace the $1 - \alpha$ quantile per direction instead with its Bonferroni-corrected $1 - \alpha/M$ quantile. While valid, this approach produces overly conservative prediction regions. We, therefore, instead tune a separate $\beta \in (\alpha/M, \alpha)$ parameter via binary search, finding the maximum β^* such that using the β^* quantile per direction provides the overall desired coverage, i.e. $|\bigcap_{m=1}^M H(u_m, \tilde{q}_m(1 - \beta^*)) \cap \mathcal{S}_C^{(1)}| / N_{C_1} \in (1 - \alpha, 1 - \alpha + \epsilon)$ for some fixed, small $\epsilon > 0$. With this choice of $\{(u_m, \tilde{q}_m)\}$, we have a defined pre-ordering, whose coverage guarantees are formally stated below and proven in Appendix B.

Theorem 3.1. *Suppose $\mathcal{D}_C := \{(X_i, Y_i)\}_{i=1}^{N_C}$ and (X', Y') are exchangeable. Assume further that K maps $s_k : \mathcal{X} \times \mathcal{Y} \rightarrow \mathbb{R}$ have been defined and a composite $s(X, Y) := (s_1(X, Y), \dots, s_K(X, Y))$ is defined. Further denote by \mathcal{S}_C the evaluation of $s(X, Y)$ on \mathcal{D}_C , namely $\mathcal{S}_C := \{s(X_i, Y_i)\}_{(X_i, Y_i) \in \mathcal{D}_C}$. For some $\alpha \in (0, 1)$, given a pre-order \lesssim in \mathbb{R}^K induced by a collection of nested sets $\{\mathcal{A}_t\}_{t \geq 0}$ define $\mathcal{Q}(\alpha) = \{s \in \mathbb{R}^K : s \lesssim s_{\lceil (N_C+1)(1-\alpha) \rceil}\}$. Then, denoting $\mathcal{C}(X) := \{y : s(X, y) \in \mathcal{Q}(\alpha)\}$, $\mathcal{P}_{X, Y}(Y' \in \mathcal{C}(X')) \geq 1 - \alpha$.*

To compute \hat{q} , for each $s \in \mathcal{S}_C^{(2)}$, we find $t^*(s)$, defined to be $\min\{t \in \mathbb{R} : s \in \bigcap_{m=1}^M H(u_m, t\tilde{q}_m)\}$. This can be efficiently computed as $t^*(s) = \max_{m=1, \dots, M} (u_m^\top s / \tilde{q}_m)$. Denoting the $\lceil (N_{C_2} + 1)(1 - \alpha) \rceil$ -th largest $t^*(s)$ as \hat{t} , $\hat{q}_m := \hat{t}\tilde{q}_m$ and $\hat{\mathcal{Q}} := \bigcap_{m=1}^M H(u_m, \hat{q}_m)$. Note that, if the tightest quantile envelope was already discovered over $\mathcal{S}_C^{(1)}$, this adjustment factor $\hat{t} \approx 1$.

Importantly, while the aforementioned procedure will necessarily result in convex regions $\hat{\mathcal{Q}}(\alpha)$, this does **not** mean the downstream prediction regions in \mathcal{Y} will be convex, discussed more fully in Section 3.3. Such flexibility is necessary, as many studies have demonstrated the need for nonconvex prediction regions for downstream utility, such as [26, 49, 47]. However, it is unsurprising such flexibility exists, as even a single *scalar* score $s_1(x, y)$ can produce nonconvex prediction regions.

Another point to emphasize is that this procedure does **not** require a fusion algorithm to be defined: this is a key conceptual separation between MVCP and traditional conformal prediction. In the classic approach, a fused predictor is conformalized; here, instead, the conformalized predictors are fused. As a result, there is *no* notion of a point prediction for MVCP: it *only* returns prediction regions. This is fundamentally unlike the traditional case, where a point prediction $\hat{y} := \mathcal{F}(x)$ is “wrapped around” by a surrounding prediction region. We present the full algorithm in Algorithm 1 and an accompanying visual walkthrough of the procedure in Appendix A.

Algorithm 1 MVCP: UNIFHYPERSPHERE(K) is a subroutine that samples $\sim \text{Unif}(\mathcal{S}^{K-1})$.

Inputs: Score functions $s_1, \dots, s_K : \mathcal{X} \rightarrow \mathcal{Y}$, Calibration set \mathcal{D}_C , Desired coverage $1 - \alpha$

- 1: $[\beta_{\text{lo}}, \beta_{\text{hi}}] \leftarrow [\alpha/M, \alpha]$, $\hat{\mathcal{Q}} \leftarrow \emptyset$, $\mathcal{S}_C^{(1)} \cup \mathcal{S}_C^{(2)} \leftarrow \{(s_1(x_i, y_i), \dots, s_K(x_i, y_i))\}_{i=1, N_{C_1}+1}^{N_{C_1}, N_{C_2}}$
- 2: $\{u_m \leftarrow \text{UNIFHYPERSPHERE}(K)\}_{m=1}^M$
- 3: **while** $|\mathcal{S}_C^{(1)} \cap \hat{\mathcal{Q}}|/N_{C_1} \notin 1 - \alpha \pm \epsilon$ **do**
- 4: $\beta \leftarrow \frac{\beta_{\text{lo}} + \beta_{\text{hi}}}{2}$
- 5: $\{\tilde{q}_m \leftarrow \frac{\lceil (N_{C_1} + 1)(1 - \beta) \rceil}{N_{C_1}} \text{ quantile of } \{u_m^\top s_i\}_{i=1}^{N_{C_1}}\}_{m=1}^M$
- 6: $\hat{\mathcal{Q}} \leftarrow \bigcap_{m=1}^M H(u_m, \tilde{q}_m)$
- 7: **if** $|\mathcal{S}_C^{(1)} \cap \hat{\mathcal{Q}}|/N_{C_1} > 1 - \alpha$ **then** $\beta_{\text{lo}} \leftarrow \beta$
- 8: **else** $\beta_{\text{hi}} \leftarrow \beta$
- 9: $\hat{t} \leftarrow \frac{\lceil (N_{C_2} + 1)(1 - \alpha) \rceil}{N_{C_2}}$ quantile of $\{\max_{m=1, \dots, M} (u_m^\top s_i / \tilde{q}_m)\}_{i=1}^{N_{C_2}}$
- 10: **Return** $\{(u_m, \hat{t}\tilde{q}_m)\}_{m=1}^M$

3.3 MVCP: Prediction Region Definition

With this generalization of the score function, a natural question is how to leverage the resulting prediction regions $\mathcal{C}(x)$. For both classification and regression, $\mathcal{C}(x) = \{y \mid s(x, y) \in \hat{\mathcal{Q}}\}$, or $\mathcal{C}(x) = \bigcap_{m=1}^M \mathcal{C}_m(x)$ where $\mathcal{C}_m(x) := \{y \mid u_m^\top s(x, y) \leq \hat{q}_m\}$.

In the *classification* setting, where $|\mathcal{Y}| \in \mathbb{N}$, explicit construction of $\mathcal{C}(x)$ is straightforward. For a fixed x , explicitly constructing $\mathcal{C}(x)$ can be done by iterating through $y \in \mathcal{Y}$ and checking if $s(x, y) \in \hat{\mathcal{Q}}$ by comparing $s(x, y)$ against each one of the defining hyperplanes after projection.

In the case of regression, however, the prediction region cannot be explicitly constructed in the general case, since \mathcal{Y} contains uncountably many elements. In fact, explicit construction is generally not of interest for downstream regression applications. Instead, prediction regions in regression settings are often simply used in their implicit form. We, therefore, focus on one particular application, namely that of [26] discussed in Section 2.2, and demonstrate the MVCP prediction regions can be leveraged in their framework. Such an extension has natural applications to the settings discussed in this original study. For instance, the authors demonstrated their method in a robust traffic routing setting with c being predicted traffic from a probabilistic weather model $q(C \mid X)$ for weather covariates X . A multiview application, therefore, naturally emerges with having separately tailored predictive models, such as another $q_2(C \mid X_2)$ predicting traffic based on historical traffic trends.

The original study demonstrated that solving this problem in a computationally efficient manner is feasible by leveraging Danskin’s Theorem so long as $\max_{\hat{c} \in \mathcal{C}(x)} f(w, \hat{c})$ is efficiently computable for any fixed w . We focus on demonstrating that this remains the case for MVCP, specifically considering the case where individual view score functions take the form of a generalization of the “GPCP” score from [26]. Let $q_k(C \mid X_k)$ represent a generative predictor for view k and

$\{\widehat{c}_{jk}\}_{j=1}^{J_k} \sim q_k(C | X_k)$ be drawn samples. Note that J_k need not be constant across k . Then, we define the score to be

$$s_k(x, c) = \min_j [g_k(\widehat{c}_{jk}, c)], \quad (3)$$

where $g_k(\widehat{c}, c)$ is any function that is convex in c for a fixed \widehat{c} . Notably this framework subsumes many standard regression settings, e.g., for a deterministic predictor, one can take $q_k(C | X_k) = \delta(f_k(X_k))$. To now compute $\max_{\widehat{c} \in \mathcal{C}(x)} f(w, \widehat{c})$, we first let $\vec{j} \in \mathcal{J} = \{j_1, \dots, j_K\}$ be an indexing tuple, where each $j_k \in \{1, \dots, J_k\}$. That is, each \vec{j} is a vector that “selects” one sample per view. Notably then, the projection $u_m^\top s(\widehat{c}_{\vec{j}}, c)$ is convex in c , since the projection directions are all restricted to \mathcal{S}_+^{K-1} . As a result, we can compute the maximizer c^* , since

$$c_{\vec{j}}^* := \arg \max_c f(w, c) \quad \text{s.t.} \quad u_m^\top s(\widehat{c}_{\vec{j}}, c) \leq \widehat{q}_m \forall m \in \{1, \dots, M\} \quad (4)$$

remains a standard convex optimization problem. The final maximum can then be found by aggregation, namely $c^* = \arg \max_{\vec{j} \in \mathcal{J}} f(w, c_{\vec{j}}^*)$. While $|\mathcal{J}| = \prod_{k=1}^K J_k$, we note that most cases of late-stage fusion in practice tend to have a limited number of views, most typically $K = 2$ or $K = 3$. This coupled with the fact that computing over these indices is trivially parallelizable means this approach is still computationally tractable. The full procedure is outlined in Algorithm 2.

Algorithm 2 Predict-Then-Optimize Under MVCP Prediction Regions

Inputs: Context x , CGMs $\{q_k(C | X_k)\}_{k=1}^K$, Optimization steps T , Sample counts $\{J_k\}_{k=1}^K$, MVCP quantile $\widehat{\mathcal{Q}} := \{(u_m, \widehat{q}_m)\}_{m=1}^M$

- 1: $w \sim U(\mathcal{W}), \{\{\widehat{c}_{jk}\}_{j=1}^{J_k}\}_{k=1}^K, \mathcal{J} = \prod_{k=1}^K [J_k]$
- 2: **for** $t \in \{1, \dots, T\}$ **do**
- 3: $\left\{ c_{\vec{j}}^* \leftarrow \arg \max_c \left\{ f(w, c) \mid u_m^\top s(\widehat{c}_{\vec{j}}, c) \leq \widehat{q}_m \forall m \in \{1, \dots, M\} \right\} \right\}_{\vec{j} \in \mathcal{J}}$
- 4: $c^* \leftarrow \arg \max_{c_{\vec{j}}^*} f(w, c_{\vec{j}}^*)$
- 5: $w \leftarrow \Pi_{\mathcal{W}}(w - \eta \nabla_w f(w, c^*))$
- 6: **Return** w

4 Experiments

We now study MVCP empirically across several tasks, demonstrating its improvement over alternate approaches in a synthetic classification task (Section 4.1), in predict-then-optimize tasks (Section 4.2), and in a classification task over a non-synthetic dataset of interest, namely Handwritten [50] (Section 4.3). To allow for fair comparison, we note that the predictors and calibration and test sets were fixed across choices of calibration procedure for each experiment. This in turn means that some care had to be taken in partitioning $\mathcal{D}_c = \mathcal{D}_c^{(1)} \cup \mathcal{D}_c^{(2)}$ for MVCP, where an insufficiently large $\mathcal{D}_c^{(1)}$ would result in poor estimation of the α -quantile envelope and hence require a large adjustment \hat{t} factor and an insufficiently large $\mathcal{D}_c^{(2)}$ in the classical reduced predictive efficiency from conformal prediction. For this reason, we fixed the split to be 20%-80% in experiments. Further details are provided in Appendix E, and code is available at: <https://github.com/yashpate15400/fusioncp>

4.1 Synthetic Classification Task

We first consider a synthetic classification task, fitting multinomial logistic regression models $\widehat{f}_k : \mathcal{X}_k \rightarrow \mathcal{Y}$, where $\mathcal{X} = \mathbb{R}^{120}$ and $\mathcal{Y} = \{1, \dots, 20\}$. We consider K -view classification problems, with $K \in \{2, \dots, 6\}$, where the views here partition the input dimension into subspaces of dimension $120/K$, namely $\mathcal{X}_i = \mathbb{R}^{1+(d/K)(i-1):(d/K)i}$ for $i \in \{1, \dots, K\}$. We compare MVCP to four baselines: a fusion-free approach that conformalizes the view with the highest predictive accuracy; an approach using a predefined “Norm” fusion algorithm as described in Section 3.1, namely with $g_1(s) = (\sum_{k=1}^K s_k^2)^{1/2}$; another similarly using a predefined “Sum” fusion algorithm with $g_2(s) = \sum_{k=1}^K s_k$; and one that conformalizes a fused predictor as also discussed in Section 3.1, with $\mathcal{F} = (\widehat{f}_1(x) + \dots + \widehat{f}_K(x))/K$. We perform conformalization using the standard classification score function across all approaches, namely $s_k(x, y) = \sum_{j=1}^l \widehat{f}_k(x)_{\pi_j(x, k)}$ where $y = \pi_l(x, k)$ and $\pi(x, k)$ is the permutation of $\{1, \dots, 20\}$ that sorts $\widehat{f}_k(x)$ from most likely to least likely. The results are presented in Table 1.

Table 1: Coverages across tasks for $\alpha = 0.10$ are shown in the left table, where coverage was assessed over a batch of 300 i.i.d. test samples. Average prediction set sizes are shown in the right table, averaged over a batch of 300 i.i.d. test samples with standard deviations in parentheses.

K	Best View	Pre-Fused	Sum	Norm	MVCP	Best View	Pre-Fused	Sum	Norm	MVCP
2	0.89	0.91	0.91	0.91	0.90	10.84 (0.34)	8.11 (0.56)	8.73 (0.42)	8.72 (0.42)	7.58 (0.42)
3	0.89	0.91	0.91	0.91	0.90	12.36 (0.30)	8.49 (0.44)	9.05 (0.32)	8.83 (0.35)	7.68 (0.42)
4	0.89	0.91	0.90	0.90	0.91	13.32 (0.30)	8.75 (0.51)	9.04 (0.47)	8.41 (0.50)	8.07 (0.50)
5	0.88	0.90	0.90	0.90	0.90	13.90 (0.19)	9.01 (0.59)	8.91 (0.63)	8.45 (0.59)	8.37 (0.58)
6	0.89	0.91	0.90	0.90	0.90	14.28 (0.27)	9.26 (0.39)	9.04 (0.68)	8.71 (0.71)	8.71 (0.75)

We see that all the approaches exhibit the desired coverage guarantees. However, the multivariate score approaches consistently produce significantly smaller prediction regions than the individually conformalized input views, with MVCP consistently producing the smallest sets on average.

4.2 MVCP Predict-Then-Optimize

We now study the use of MVCP across predict-then-optimize tasks, specifically considering the fractional knapsack problem as in the original conformal predict-then-optimize paper [26]:

$$w^*(x) := \min_w \max_{\hat{c} \in \mathcal{C}(X)} -\hat{c}^T w \quad (5)$$

$$\text{s.t. } w \in [0, 1]^n, p^T w \leq B, \mathcal{P}_{X,C}(C \in \mathcal{C}(X)) \geq 1 - \alpha,$$

where $p \in \mathbb{R}^n$ and $B > 0$. The distributions $\mathcal{P}(C)$ and $\mathcal{P}(X | C)$ are again taken to be those from various simulation-based inference (SBI) benchmark tasks provided by [51], chosen as they have $\mathcal{P}(C | X)$ with complex structure, fully described in Appendix C. We specifically study the Gaussian Mixture distributional setup across increasing dimensions to highlight the capacity for MVCP to succeed even for complex combinations of distributions.

We then consider $K = 2$ views, namely with $\mathcal{X} = \mathbb{R}^d$, $\mathcal{X}_1 = \mathbb{R}^{d_1}$, and $\mathcal{X}_2 = \mathbb{R}^{d_1+d_2}$. For each \mathcal{X}_k , we train a generative model $q_k(C | X_k)$, specifically a normalizing flow. We then compare four distinct ways of formulating $\mathcal{C}(X)$, namely by conformalizing each view individually, by conformalizing a fused map, by fusing the scores via a sum, and by fusing with MVCP, all using the score given by Equation (3), specifically taking g_k to be the ℓ^2 metric. The ‘‘Pre-fused’’ strategy employed here is again a mean aggregation, i.e. a sample $\hat{c} \sim \mathcal{F}(q_1, q_2)$ is drawn via $\hat{c}_1 \sim q_1(C | X_1)$, $\hat{c}_2 \sim q_2(C | X_2)$ and \hat{c} defined as $(\hat{c}_1 + \hat{c}_2)/2$.

As discussed in Section 3.3, the prediction regions are not explicitly constructed in regression settings, rendering the reporting of prediction region sizes impossible. We instead compare the expected suboptimality gap proportion, $\Delta_{\%} = \mathbb{E}_X[\Delta(X, C(X))/\min_w f(w, C(X))]$, where Δ is defined as discussed in Section 2.2. This quantity measures the conservatism of the produced robust optimal value and is bounded in $[0, 1]$ in this setting, with the upper bound seen as Equation (5) can trivially be solved by simply taking $w = 0$. The results are presented in Table 2.

Table 2: Coverages across tasks for $\alpha = 0.05$ are shown in the left table, where coverage was assessed over a batch of 500 i.i.d. test samples. Suboptimality gap proportions ($\Delta_{\%}$) are shown in the right table, with medians reported over a batch of 500 i.i.d. test samples and median average deviations in parentheses.

	View 1	View 2	Pre-Fused	Sum	MVCP	View 1	View 2	Pre-Fused	Sum	MVCP
Gaussian Mixture (1)	0.964	0.958	0.952	0.964	0.976	0.901 (0.1003)	0.886 (0.1144)	1.0 (0.0)	0.702 (0.1403)	0.542 (0.0946)
Gaussian Mixture (2)	0.938	0.938	0.93	0.95	0.94	0.962 (0.0453)	1.0 (0.0155)	1.005 (0.0019)	0.893 (0.1084)	0.874 (0.0792)
Gaussian Mixture (3)	0.944	0.972	0.936	0.944	0.948	1.011 (0.018)	0.997 (0.0208)	1.011 (0.0035)	0.838 (0.0735)	0.868 (0.047)
Gaussian Mixture (4)	0.942	0.94	0.914	0.95	0.924	1.026 (0.0181)	0.987 (0.0327)	1.018 (0.0066)	1.003 (0.0144)	0.946 (0.0286)

We see that all methods produce the coverage guarantees in accordance to Theorem 3.1. The resulting suboptimality gaps additionally exhibit two notable characteristics. The first is that MVCP produces more informative prediction regions, and hence less conservative robust upper bounds, if the views in consideration are individually informative, that is, each has $\Delta_{\%} < 1$. While the sum conformal fusion exhibits a similar pattern, its effective reduction is consistently less than that provided by MVCP. Additionally, in cases where one of the two views is *uninformative*, i.e. $\Delta_{\%} = 1$, MVCP nearly retains the performance of the informative view, as the quantile envelope adapts in considering all projection directions. The sum fusion technique, on the other hand, significantly degrades from the performance of the optimal view.

4.3 Real Data Classification

We now conduct experiments on the Handwritten dataset [50]. This dataset consists of features of 2000 handwritten digits (0 – 9) (200 examples per class) with 6 different views of each image extracted from a collection of Dutch utility maps, described fully in Appendix D. The baseline approaches parallel those presented in Section 4.1. The results are compiled in Table 3. As in the synthetic classification experiment, we see that considering multiple views produces significantly more informative prediction regions than solely conformalizing a single view, especially when done in the manner prescribed by MVCP.

Table 3: Coverages across tasks for $\alpha = 0.10$ are shown in the left table, where coverage was assessed over a batch of 295 i.i.d. test samples. Average prediction set sizes are shown in the right table, averaged over a batch of 295 i.i.d. test samples with standard deviations in parentheses.

K	Best View	Pre-Fused	Sum	Norm	MVCP	Best View	Pre-Fused	Sum	Norm	MVCP
2	0.90	0.91	0.91	0.91	0.90	3.39 (0.09)	3.69 (0.11)	3.52 (0.13)	3.51 (0.13)	2.68 (0.17)
3	0.90	0.90	0.90	0.90	0.90	3.39 (0.09)	3.48 (0.09)	2.97 (0.09)	2.95 (0.09)	1.84 (0.10)
4	0.91	0.90	0.90	0.90	0.90	3.28 (0.14)	3.42 (0.05)	2.87 (0.05)	2.83 (0.05)	1.64 (0.12)
5	0.91	0.91	0.91	0.90	0.90	3.28 (0.14)	3.12 (0.07)	2.73 (0.08)	2.68 (0.07)	1.55 (0.06)
6	0.90	0.91	0.90	0.90	0.91	3.19 (0.17)	3.07 (0.11)	2.71 (0.06)	2.64 (0.05)	1.60 (0.07)

5 Discussion

We have presented MVCP, a framework for producing informative prediction regions in late-stage fusion pipelines. We additionally demonstrated the generality of the proposed pipeline in settings of both classification and robust predict-then-optimize regression tasks. This work suggests many directions for extension. One point of interest is the integration of MVCP with other downstream regression applications. For instance, [52] proposed an end-to-end differentiable extension to [26]; extending MVCP for integration to their framework would be of great interest. Additionally, given the prevalence of late-stage fusion in robotics applications, an exciting applied avenue of research would investigate the optimization of MVCP to leverage it in settings of robust control.

6 Acknowledgements

We acknowledge the support of the College of Literature, Science, and the Arts at the University of Michigan via the Meet the Moment Research Initiative.

References

- [1] Lvmin Zhang, Anyi Rao, and Maneesh Agrawala. Adding conditional control to text-to-image diffusion models. In *Proceedings of the IEEE/CVF International Conference on Computer Vision*, pages 3836–3847, 2023.
- [2] Alec Radford, Jong Wook Kim, Chris Hallacy, Aditya Ramesh, Gabriel Goh, Sandhini Agarwal, Girish Sastry, Amanda Askell, Pamela Mishkin, Jack Clark, et al. Learning transferable visual models from natural language supervision. In *International conference on machine learning*, pages 8748–8763. PMLR, 2021.
- [3] Shiliang Sun. A survey of multi-view machine learning. *Neural computing and applications*, 23:2031–2038, 2013.
- [4] Jing Zhao, Xijiong Xie, Xin Xu, and Shiliang Sun. Multi-view learning overview: Recent progress and new challenges. *Information Fusion*, 38:43–54, 2017.
- [5] Xiaoqiang Yan, Shizhe Hu, Yiqiao Mao, Yangdong Ye, and Hui Yu. Deep multi-view learning methods: A review. *Neurocomputing*, 448:106–129, 2021.
- [6] Ye Yuan, Guangxu Xun, Kebin Jia, and Aidong Zhang. A multi-view deep learning framework for eeg seizure detection. *IEEE journal of biomedical and health informatics*, 23(1):83–94, 2018.
- [7] Yifeng Li, Fang-Xiang Wu, and Alioune Ngom. A review on machine learning principles for multi-view biological data integration. *Briefings in bioinformatics*, 19(2):325–340, 2018.
- [8] Ye Yuan, Guangxu Xun, Kebin Jia, and Aidong Zhang. A multi-view deep learning method for epileptic seizure detection using short-time fourier transform. In *Proceedings of the 8th ACM international conference on bioinformatics, computational biology, and health informatics*, pages 213–222, 2017.
- [9] Xiangjun Wu, Hui Hui, Meng Niu, Liang Li, Li Wang, Bingxi He, Xin Yang, Li Li, Hongjun Li, Jie Tian, et al. Deep learning-based multi-view fusion model for screening 2019 novel coronavirus pneumonia: a multicentre study. *European Journal of Radiology*, 128:109041, 2020.
- [10] Ramon F Brena, Antonio A Aguilera, Luis A Trejo, Erik Molino-Minero-Re, and Oscar Mayora. Choosing the best sensor fusion method: A machine-learning approach. *Sensors*, 20(8):2350, 2020.
- [11] Erik Blasch, Tien Pham, Chee-Yee Chong, Wolfgang Koch, Henry Leung, Dave Braines, and Tarek Abdelzاهر. Machine learning/artificial intelligence for sensor data fusion—opportunities and challenges. *IEEE Aerospace and Electronic Systems Magazine*, 36(7):80–93, 2021.
- [12] Mary B Alatise and Gerhard P Hancke. A review on challenges of autonomous mobile robot and sensor fusion methods. *IEEE Access*, 8:39830–39846, 2020.
- [13] De Jong Yeong, Gustavo Velasco-Hernandez, John Barry, and Joseph Walsh. Sensor and sensor fusion technology in autonomous vehicles: A review. *Sensors*, 21(6):2140, 2021.
- [14] Venice Erin Liong, Thi Ngoc Tho Nguyen, Sergi Widjaja, Dhananjai Sharma, and Zhuang Jie Chong. Amvnet: Assertion-based multi-view fusion network for lidar semantic segmentation. *arXiv preprint arXiv:2012.04934*, 2020.
- [15] Zongbo Han, Changqing Zhang, Huazhu Fu, and Joey Tianyi Zhou. Trusted multi-view classification with dynamic evidential fusion. *IEEE transactions on pattern analysis and machine intelligence*, 45(2):2551–2566, 2022.
- [16] Wentao Wei, Qingfeng Dai, Yongkang Wong, Yu Hu, Mohan Kankanhalli, and Weidong Geng. Surface-electromyography-based gesture recognition by multi-view deep learning. *IEEE Transactions on Biomedical Engineering*, 66(10):2964–2973, 2019.
- [17] Tongxin Wang, Wei Shao, Zhi Huang, Haixu Tang, Jie Zhang, Zhengming Ding, and Kun Huang. Mogonet integrates multi-omics data using graph convolutional networks allowing patient classification and biomarker identification. *Nature Communications*, 12(1):3445, 2021.
- [18] Mahesh Subedar, Ranganath Krishnan, Paulo Lopez Meyer, Omesh Tickoo, and Jonathan Huang. Uncertainty-aware audiovisual activity recognition using deep bayesian variational inference. In *Proceedings of the IEEE/CVF international conference on computer vision*, pages 6301–6310, 2019.
- [19] Junjiao Tian, Wesley Cheung, Nathaniel Glaser, Yen-Cheng Liu, and Zsolt Kira. Uno: Uncertainty-aware noisy-or multimodal fusion for unanticipated input degradation. In *2020 IEEE International Conference on Robotics and Automation (ICRA)*, pages 5716–5723. IEEE, 2020.
- [20] John Denker and Yann LeCun. Transforming neural-net output levels to probability distributions. *Advances in neural information processing systems*, 3, 1990.

- [21] Marton Havasi, Rodolphe Jenatton, Stanislav Fort, Jeremiah Zhe Liu, Jasper Snoek, Balaji Lakshminarayanan, Andrew M Dai, and Dustin Tran. Training independent subnetworks for robust prediction. *arXiv preprint arXiv:2010.06610*, 2020.
- [22] Andrey Malinin and Mark Gales. Predictive uncertainty estimation via prior networks. *Advances in neural information processing systems*, 31, 2018.
- [23] Anastasios N Angelopoulos and Stephen Bates. A gentle introduction to conformal prediction and distribution-free uncertainty quantification. *arXiv preprint arXiv:2107.07511*, 2021.
- [24] Glenn Shafer and Vladimir Vovk. A tutorial on conformal prediction. *Journal of Machine Learning Research*, 9(3), 2008.
- [25] Jesse C Cresswell, Yi Sui, Bhargava Kumar, and Noël Vouitsis. Conformal prediction sets improve human decision making. *arXiv preprint arXiv:2401.13744*, 2024.
- [26] Yash Patel, Sahana Rayan, and Ambuj Tewari. Conformal contextual robust optimization. *arXiv preprint arXiv:2310.10003*, 2023.
- [27] Shunichi Ohmori. A predictive prescription using minimum volume k-nearest neighbor enclosing ellipsoid and robust optimization. *Mathematics*, 9(2):119, 2021.
- [28] Abhilash Reddy Chenreddy, Nymisha Bandi, and Erick Delage. Data-driven conditional robust optimization. *Advances in Neural Information Processing Systems*, 35:9525–9537, 2022.
- [29] Chunlin Sun, Linyu Liu, and Xiaocheng Li. Predict-then-calibrate: A new perspective of robust contextual lp. *arXiv preprint arXiv:2305.15686*, 2023.
- [30] Guoqing Chao, Shiliang Sun, and Jinbo Bi. A survey on multiview clustering. *IEEE transactions on artificial intelligence*, 2(2):146–168, 2021.
- [31] Weiran Wang, Raman Arora, Karen Livescu, and Jeff Bilmes. On deep multi-view representation learning. In *International conference on machine learning*, pages 1083–1092. PMLR, 2015.
- [32] Chong Wang. Variational bayesian approach to canonical correlation analysis. *IEEE Transactions on Neural Networks*, 18(3):905–910, 2007.
- [33] Galen Andrew, Raman Arora, Jeff Bilmes, and Karen Livescu. Deep canonical correlation analysis. In *International conference on machine learning*, pages 1247–1255. PMLR, 2013.
- [34] Weiran Wang, Xinchun Yan, Honglak Lee, and Karen Livescu. Deep variational canonical correlation analysis. *arXiv preprint arXiv:1610.03454*, 2016.
- [35] Philip Bachman, R Devon Hjelm, and William Buchwalter. Learning representations by maximizing mutual information across views. *Advances in neural information processing systems*, 32, 2019.
- [36] Douwe Kiela, Edouard Grave, Armand Joulin, and Tomas Mikolov. Efficient large-scale multi-modal classification. In *Proceedings of the AAAI conference on artificial intelligence*, volume 32, 2018.
- [37] Xinwang Liu, Xinzhong Zhu, Miaomiao Li, Lei Wang, Chang Tang, Jianping Yin, Dinggang Shen, Huaimin Wang, and Wen Gao. Late fusion incomplete multi-view clustering. *IEEE transactions on pattern analysis and machine intelligence*, 41(10):2410–2423, 2018.
- [38] Siwei Wang, Xinwang Liu, En Zhu, Chang Tang, Jiyuan Liu, Jingtao Hu, Jingyuan Xia, and Jianping Yin. Multi-view clustering via late fusion alignment maximization. In *IJCAI*, pages 3778–3784, 2019.
- [39] Siwei Wang, Xinwang Liu, Li Liu, Sihang Zhou, and En Zhu. Late fusion multiple kernel clustering with proxy graph refinement. *IEEE Transactions on Neural Networks and Learning Systems*, 2021.
- [40] Tiejian Zhang, Xinwang Liu, Lei Gong, Siwei Wang, Xin Niu, and Li Shen. Late fusion multiple kernel clustering with local kernel alignment maximization. *IEEE Transactions on Multimedia*, 2021.
- [41] Emilie Morvant, Amaury Habrard, and Stéphane Ayache. Majority vote of diverse classifiers for late fusion. In *Structural, Syntactic, and Statistical Pattern Recognition: Joint IAPR International Workshop, S+ SSPR 2014, Joensuu, Finland, August 20-22, 2014. Proceedings*, pages 153–162. Springer, 2014.
- [42] Peter J Rousseeuw and Anja Struyf. Computing location depth and regression depth in higher dimensions. *Statistics and Computing*, 8:193–203, 1998.
- [43] Robert Serfling. Quantile functions for multivariate analysis: approaches and applications. *Statistica Neerlandica*, 56(2):214–232, 2002.
- [44] Linglong Kong and Ivan Mizera. Quantile tomography: Using quantiles with multivariate data. *Statistica Sinica*, pages 1589–1610, 2012.

- [45] Davy Paindaveine and Miroslav Šiman. On directional multiple-output quantile regression. *Journal of Multivariate Analysis*, 102(2):193–212, 2011.
- [46] Marc Hallin, Davy Paindaveine, and Marianna Šiman. Multivariate quantiles and multiple-output regression quantiles: From ℓ_1 optimization to halfspace depth. *Annals of Statistics*, 38:635–669, 2010.
- [47] Shai Feldman, Stephen Bates, and Yaniv Romano. Calibrated multiple-output quantile regression with representation learning. *Journal of Machine Learning Research*, 24(24):1–48, 2023.
- [48] Stefan Schnabel and Wolfhard Janke. A simple algorithm for uniform sampling on the surface of a hypersphere. *arXiv preprint arXiv:2204.14004*, 2022.
- [49] Renukanandan Tumu, Matthew Cleaveland, Rahul Mangharam, George J Pappas, and Lars Lindemann. Multimodal conformal prediction regions by optimizing convex shape templates. *arXiv preprint arXiv:2312.07434*, 2023.
- [50] Robert Duin. Multiple Features. UCI Machine Learning Repository. DOI: <https://doi.org/10.24432/C5HC70>.
- [51] Joeri Hermans, Arnaud Delaunoy, François Rozet, Antoine Wehenkel, and Gilles Louppe. Averting a crisis in simulation-based inference. *arXiv preprint arXiv:2110.06581*, 2021.
- [52] Abhilash Chenreddy and Erick Delage. End-to-end conditional robust optimization. *arXiv preprint arXiv:2403.04670*, 2024.
- [53] Jan-Matthis Lueckmann, Jan Boelts, David Greenberg, Pedro Goncalves, and Jakob Macke. Benchmarking simulation-based inference. In *International Conference on Artificial Intelligence and Statistics*, pages 343–351. PMLR, 2021.
- [54] Adam Paszke, Sam Gross, Francisco Massa, Adam Lerer, James Bradbury, Gregory Chanan, Trevor Killeen, Zeming Lin, Natalia Gimelshein, Luca Antiga, et al. Pytorch: An imperative style, high-performance deep learning library. *Advances in Neural Information Processing Systems*, 32, 2019.
- [55] Conor Durkan, Artur Bekasov, Iain Murray, and George Papamakarios. nflows: normalizing flows in PyTorch, November 2020.
- [56] Diederik P Kingma and Jimmy Ba. Adam: A method for stochastic optimization. *arXiv preprint arXiv:1412.6980*, 2014.

A Multivariate Visualization

We walk through a visual presentation of the approach below to supplement the textual description in the main text. As discussed, we start with a collection of multivariate calibration scores \mathcal{S}_C with $s \in \mathcal{S}$ being $\in \mathbb{R}^K$. For the purposes of visualization in this section, we have $K = 2$. We first partition the score evaluations $\mathcal{S}_C = \mathcal{S}_C^{(1)} \cup \mathcal{S}_C^{(2)}$ into a subset used to define the pre-ordering and the remainder to define the multivariate quantile.

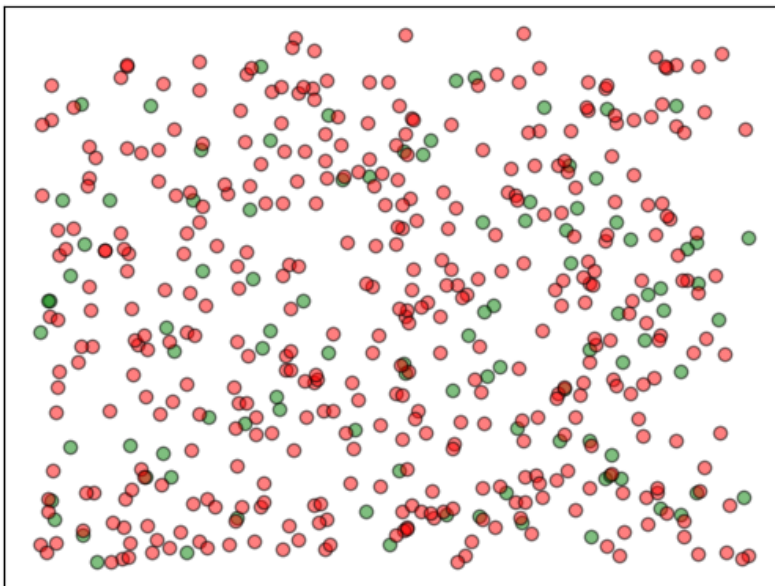


Figure 2: The calibration score evaluations are first split between those used to define the pre-ordering (green) and those used to define the final multivariate quantile (red).

We first wish to define the pre-ordering over $\mathcal{S}_C^{(1)}$. As described in the main text, the goal is to define this using an indexed family of sets \mathcal{A}_t with index $t \in \mathbb{R}$, after which the multivariate quantile reduces to the univariate quantile formulation. To ensure the final envelope over $\mathcal{S}_C^{(2)}$ remains as tight as possible, we wish to define this family in a data-driven fashion. Critically, the *shape* of this tightest envelope around $\mathcal{S}_C^{(2)}$ will vary across α , meaning we must define the family *separately* for each choice of α . We expect the contour of the tightest α envelope for $\mathcal{S}_C^{(1)}$ will be similar to that over $\mathcal{S}_C^{(2)}$, motivating such a choice to define the indexing family. To do this, we project $\mathcal{S}_C^{(1)}$ along a number of directions, finding the β quantile along each, in turn defining a half-plane, where β is as described in Section 3.2.

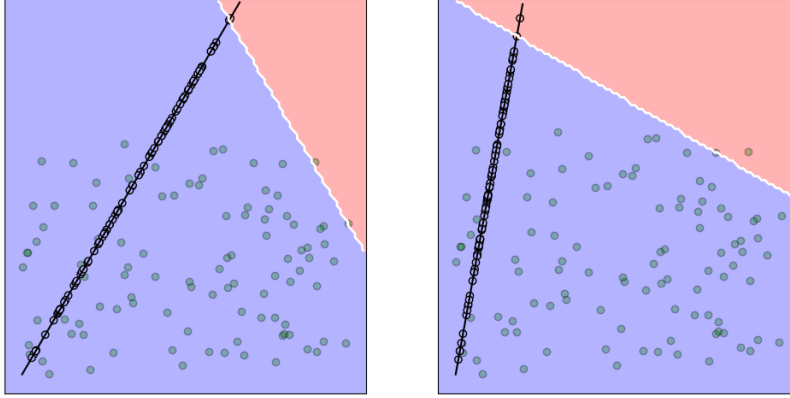


Figure 3: The pre-ordering points are projected across a number of directions, after which the β quantile is used to define a direction quantile. This defines a half-plane of points that are in the region (blue) and those outside (red).

We then iteratively update β in the manner described in Algorithm 1 to obtain β^* , namely the minimum value for which the region given by the intersection of the corresponding half-planes covers roughly $1 - \alpha$ of $\mathcal{S}_C^{(1)}$.

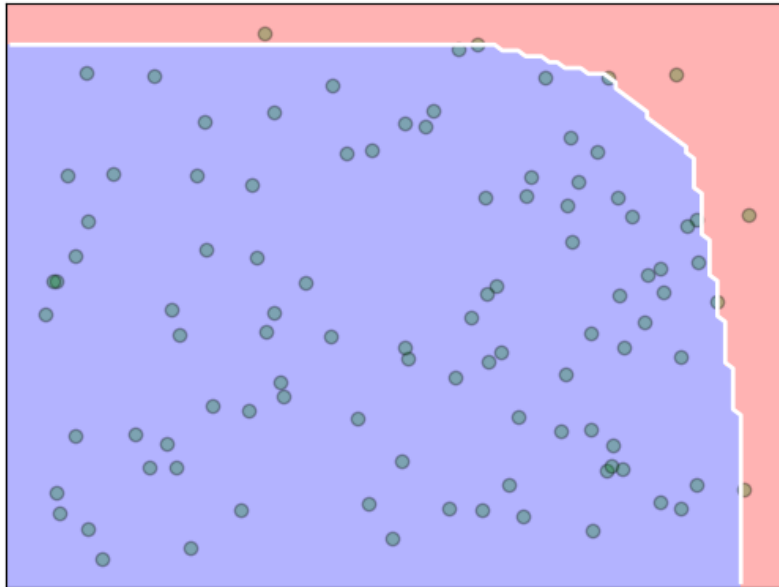


Figure 4: We use the intersection of hyperplanes to define the quantile envelope, seeking β^* that achieves the desired coverage.

Once this $1 - \alpha$ quantile envelope of $\mathcal{S}_C^{(1)}$ is found, we define \mathcal{A}_1 to be such an envelope, with which future points can now be partially ordered. That is, for any point $s \in \mathbb{R}^K$ notice that we can unambiguously associate it with $t(s) := \min\{t \in \mathbb{R} : s \in \mathcal{A}_t\}$. Intuitively, this is the t where the contour “intersects” s . Notably, now that the partial ordering has been defined, the points of $\mathcal{S}_C^{(1)}$ are no longer used. It would be of interest to investigate whether a concurrent definition of the partial ordering and final calibration is possible without such data splitting in future work.

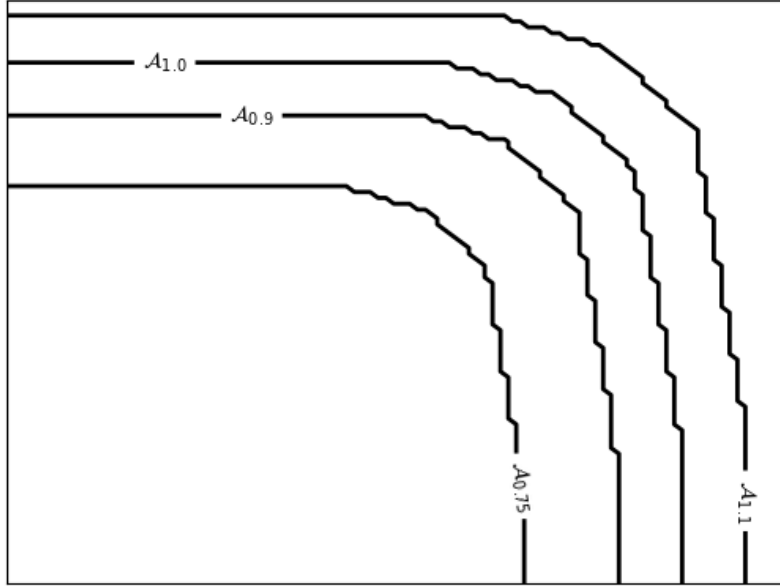


Figure 5: Using the quantile envelope, the family of nested sets \mathcal{A}_t is defined, in turn defining a partial ordering over \mathbb{R}^K .

With this \mathcal{A}_t , we find the final \hat{q} simply by mapping the points of $\mathcal{S}_C^{(2)}$ to their corresponding $t(s)$ values in the aforementioned fashion and performing standard conformal prediction. As discussed, if the envelope has a similar structure to that found over $\mathcal{S}_C^{(1)}$, the envelope should be adjusted by only a minor amount.

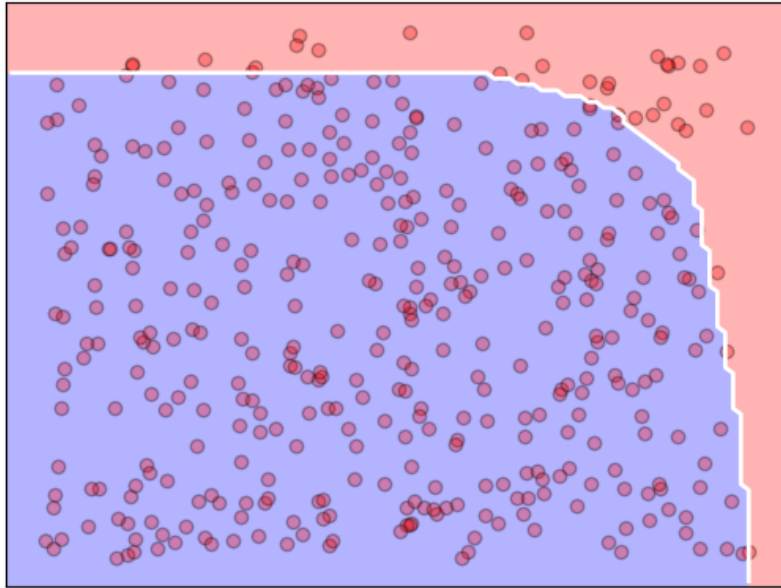


Figure 6: Using the nested family of sets, we expand or contract the envelope appropriately using the data of $\mathcal{S}_C^{(2)}$ to find the final adjustment factor.

B Multivariate Score Coverage

The proof of the multivariate extension of conformal prediction follows in precisely the same manner as that of standard conformal prediction with the pre-order \lesssim replacing the complete ordering used in traditional conformal prediction.

Theorem B.1. Suppose $\mathcal{D}_C := \{(X_i, Y_i)\}_{i=1}^{N_C}$ and (X', Y') are exchangeable. Assume further that K maps $s_j : \mathcal{X} \times \mathcal{Y} \rightarrow \mathbb{R}$ have been defined and a composite $s(X, Y) := (s_1(X, Y), \dots, s_K(X, Y))$ is defined. Further denote by \mathcal{S}_C the evaluation of $s(X, Y)$ on \mathcal{D}_C , namely $\mathcal{S}_C := \{s(X_i, Y_i)\}_{(X_i, Y_i) \in \mathcal{D}_C}$. For some $\alpha \in (0, 1)$, given a pre-order \lesssim in \mathbb{R}^K define $\mathcal{Q}(\alpha) = \{s \in \mathbb{R}^K : s \lesssim s_{\lceil (N_C+1)(1-\alpha) \rceil}\}$. Then, denoting $\mathcal{C}(X) := \{y : s(X, y) \in \mathcal{Q}(\alpha)\}$,

$$\mathcal{P}_{X,Y}(Y' \in \mathcal{C}(X')) \geq 1 - \alpha. \quad (6)$$

Proof. Denote $s_i = s(X_i, Y_i)$ for each $i = 1, \dots, n$ and $s' = s(X', Y')$. We define $t_i = \inf\{t \geq 0 : s_i \in \mathcal{A}_t\}$ and $t' = \inf\{t \geq 0 : s' \in \mathcal{A}_t\}$. We consider the case that $\mathcal{P}_{X,Y}(t_i \neq t_j) = 1$, that is, that the probability of ties is a probability measure 0 set. Without loss of generality, we then assume the scores are sorted according to the assumed pre-order, namely that $s_1 \lesssim s_2 \lesssim \dots \lesssim s_{N_C}$, or equivalently $t_1 \leq t_2 \leq \dots \leq t_{N_C}$. We then again have that $\hat{t} = t_{\lceil (N_C+1)(1-\alpha) \rceil}$ if $\alpha > 1/(N_C + 1)$ and $\hat{t} = \infty$ otherwise. In the latter case, coverage is trivially satisfied. In the former case, we see

$$\mathcal{P}_{X,Y}(Y' \in \mathcal{C}(X')) = \mathcal{P}_{X,Y}(s(X, y) \lesssim s_{\lceil (N_C+1)(1-\alpha) \rceil}) = \mathcal{P}_{X,Y}(t' \leq t_{\lceil (N_C+1)(1-\alpha) \rceil}). \quad (7)$$

By the assumed exchangeability of $\mathcal{D}_C := \{(X_i, Y_i)\}_{i=1}^{N_C}$ and (X', Y') , we have that

$$\mathcal{P}_{X,Y}(t' \leq t_k) = \frac{k}{N_C + 1}, \quad (8)$$

for any k . From here, we have the desired conclusion that

$$\mathcal{P}_{X,Y}(s(X, y) \lesssim s_{\lceil (N_C+1)(1-\alpha) \rceil}) = \left(\frac{1}{N_C + 1}\right) (\lceil (N_C + 1)(1 - \alpha) \rceil) \geq 1 - \alpha, \quad (9)$$

completing the proof as desired. \square

C Simulation-Based Inference Benchmarks

The benchmark tasks are a subset of those provided by [53]. For convenience, we provide brief descriptions of the tasks curated by this library; however, a more comprehensive description of these tasks can be found in their manuscript.

C.1 Gaussian Mixture

A mixture of two Gaussians, with one having a much broader covariance structure:

$$\text{Prior: } \beta \sim \mathcal{U}(-10, 10)$$

$$\text{Simulator: } x \mid w \sim 0.5\mathcal{N}(x \mid w, I) + 0.5\mathcal{N}(x \mid w, .01I)$$

For any Gaussian Mixture (k) distribution referenced in Section 4, we combined separate instances of this setup, where the typical setup has $\beta \in \mathbb{R}^2$. In other words, we generate $x := [x_1, \dots, x_k]$ by drawing a prior over a similarly partitioned $\theta := [\theta_1, \dots, \theta_k]$ and taking $x_i \sim \mathcal{P}(X_i \mid \theta_i)$ according to the above distribution.

D Real Data Featurization

The data features of the Handwritten dataset [50] are as follow:

- 47 Zernike moments
- 76 Fourier coefficients of the character shapes
- 6 morphological features
- 240 pixel averages in 2×3 windows
- 64 Karhunen-Love coefficients
- 216 profile correlations

E Training Details

All encoders were implemented in PyTorch [54] with a Neural Spline Flow architecture. The NSF was built using code from [55]. Specific architecture hyperparameter choices were taken to be the defaults from [55] and are available in the code. Optimization was done using Adam [56] with a learning rate of 10^{-3} over 5,000 training steps. Minibatches were drawn from the corresponding prior $\mathcal{P}(Y)$ and simulator $\mathcal{P}(X | Y)$ as specified per task in the preceding section. Training these models required between 10 minutes and two hours using an Nvidia RTX 2080 Ti GPUs for each of the SBI tasks.